Journal of Structural Geology, Vol. 15, No. 6, pp. 793 to 804, 1993
Printed in Great Britain

0191-8141/93 $06.00+0.00

Quantitative texture analysis of naturally deformed anhydrite by neutron diffraction texture goniometry

DAVID MAINPRICE

Laboratoire de Tectonophysique, Université Montpellier II, 34060 Montpellier, France

JEAN-LUC BOUCHEZ

Laboratoire de Pétrophysique, 38 rue des 36 Ponts, 31400 Toulouse, France

MARTIN CASEY

Geologisches Institut, ETH-Zentrum, CH-8092 Zurich, Switzerland

and

PIERRE DERVIN

Laboratoire Léon-Brillouin, C.E.N. Saclay, 91190 Gif-sur-Yvette, France

(*Received* 2 *January* 1991; *accepted in revised form* 14 *August* 1992)

Abstract—The crystallographic texture of coarse-grained (1 mm) foliated anhydrite from an evaporite diapir in the Canadian Arctic Islands was analysed by neutron diffraction texture goniometry. The orientation distribution function (ODF), which quantatively defines the texture, was calculated from eight pole figures. The ODF was used to calculate the pole figures for slip systems and twin planes. A strong concentration of ⊥(020) was found parallel to the lineation (*X*) with ⊥(002) forming a girdle normal to the lineation, with a strong maximum near the foliation normal (*Z*). The maxima are slightly asymmetric with respect to the structural framework (*X*–*Y*–*Z*) which is typical of non-coaxial deformation.

The orientation of ⊥(020) and ⊥(002) are consistent with [010](001) glide in a non-coaxial flow regime. The axial symmetry about the lineation (*X*) of the pole figures and the tubular structure of the ODF are thought to have been caused by an important component of extension parallel to *X*. The calculated (100) pole figure has a submaximum parallel to *Z*, presumably a direction of high compressive stress. The ⊥(101) maxima at about 45° to *Z* are then indicative of twinning on {101}. Approximately 30% of the ODF is in a twinned orientation ([100] subparallel to *Z*) and it is suggested that twinning contributed to the axial symmetry of the fabric. Few grains show undulary extinction, their boundaries are generally straight and rarely serrated. This points to extensive migration recrystallization and associated twin gliding at >300°C. Previous studies seem to have underestimated the contribution of twinning to texture development, which is dominated by [010](001) slip.

INTRODUCTION

ANHYDRITE ($CaSO_4$) is an important component in many evaporite sequences, together with halite, calcite, dolomite, gypsum and clay minerals. Two distinct tectonic settings of evaporite have been observed, namely diapirs (e.g. North German plain; Schwerdtner 1964) and detachment horizons (e.g. Jura fold belt; Jordan *et al.* 1990). In both settings the evaporites are characterized by their relatively high ductility compared with surrounding rocks. Anhydrite typically forms continuous horizons of pure material, sometimes being interlayered with clay horizons. Anhydrite transforms to gypsum ($CaSO_4.2H_2O$) within at a few hundred metres of the surface, hence the former is the mechanically important component at depth in gypsum–anhydrite sequences observed at the surface.

Evaporite diapirs are plugs or wall-like structures which may be several kilometres in extent. The diapirs move upward piercing the surrounding sediments driven by the density differences between the evaporites and the sediments. These structures have attracted the interest of geologists as the diapirs cause local folding and faulting in their surroundings, producing potential oil and gas traps. More recently such diapirs have been proposed as possible depositories for the storage of radioactive waste. The high ductility of the evaporites will enable the galleries in the diapir to seal over a short time span and in so doing isolate the radioactive material.

Relatively few fabric studies have been made of anhydrite from any tectonic setting. All the previous studies of natural deformation have been made using the traditional optical microscope equipped with a Universal stage, except for the recent study by Jordan *et al.* (1990) using X-ray pole figures. Anhydrite rocks from salt domes in north-west Germany (Lamcke 1936, Schwerdtner 1964) and the southern United States (Balk 1949) constitute all the work to-date. In deformed specimens the grains are characterized by a rectangular shape with the long axis parallel to [010] and the short axis parallel to [001] (e.g. Schwerdtner 1970). Whereas in

undeformed specimens the long axis is parallel to [100] and the short axis parallel to [010] (Ramez 1976b). Twinning on {101} is occasionally observed in naturally deformed samples (Lamcke 1936), and cleavages parallel to (010) and (001) are observed in most grains. (010) pole figures show a strong concentration parallel to lineation in all naturally deformed examples (Kern & Richter 1985, Jordan *et al.* 1990). (100) and (001) pole figures show great circle distributions normal to the lineation. Despite the presence of cleavages and occasional {101} twins, the identification of the optical orientation is difficult, time consuming, and prone to errors. Hence we have undertaken the first quantative fabric (texture) analysis using the spherical harmonic pole figure inversion method applied to pole figures measured on a neutron diffraction texture goniometer. The diffraction technique allows a truly volumetric determination of the fabric.

SAMPLE LOCATION

An oriented specimen of naturally deformed anhydrite was collected at the south-western edge of the Gibs Fiord diapir in the central Eureka Sound fold belt, Canadian Arctic islands (Fig. 1) (van Berkel *et al.* 1983). This evaporate diapir occupies the central region of an arcuate anticline, the axial trace of which is marked by the well-defined Gibs Fjord Fault. The anhydrite is finely layered parallel to a strong planar grain-shape fabric, a common feature in these anhydrite rocks. Much less common is a conspicuous grain-shape lineation clearly visible on the foliation plane. Thin sections cut from the specimen show the sample to be 95% anhydrite with minor (5%) transformation to gypsum. Grains, about 1 mm in size, have a rectangular form, being elongated parallel to [010] and defining the grain-shape lineation (Fig. 2). Grain boundaries are often straight. Most grains contain one or two twin lamellae {101}, apparently pointing to a low twinned volume fraction, and cleavages (010) and (001) were commonly observed.

GONIOMETRY AND DATA ANALYSIS

The neutron diffraction texture goniometry measurements were performed at C.E.N. Saclay (Paris, France) using a thermal neutron source with a wavelength of 0.205 nm. Pole figures were measured with an azimuthal step of 3.75° and inclination step of 5°, resulting in 1824 measurement points on a hemisphere. A powder of anhydrite was prepared from the specimen for an exploratory diagram in 2θ Bragg. The eight strongest peaks in 2θ between 0° and 90° were chosen (Fig. 3) for texture analysis. Pole figures were measured over a total counting time of approximately 48 h for each of the eight

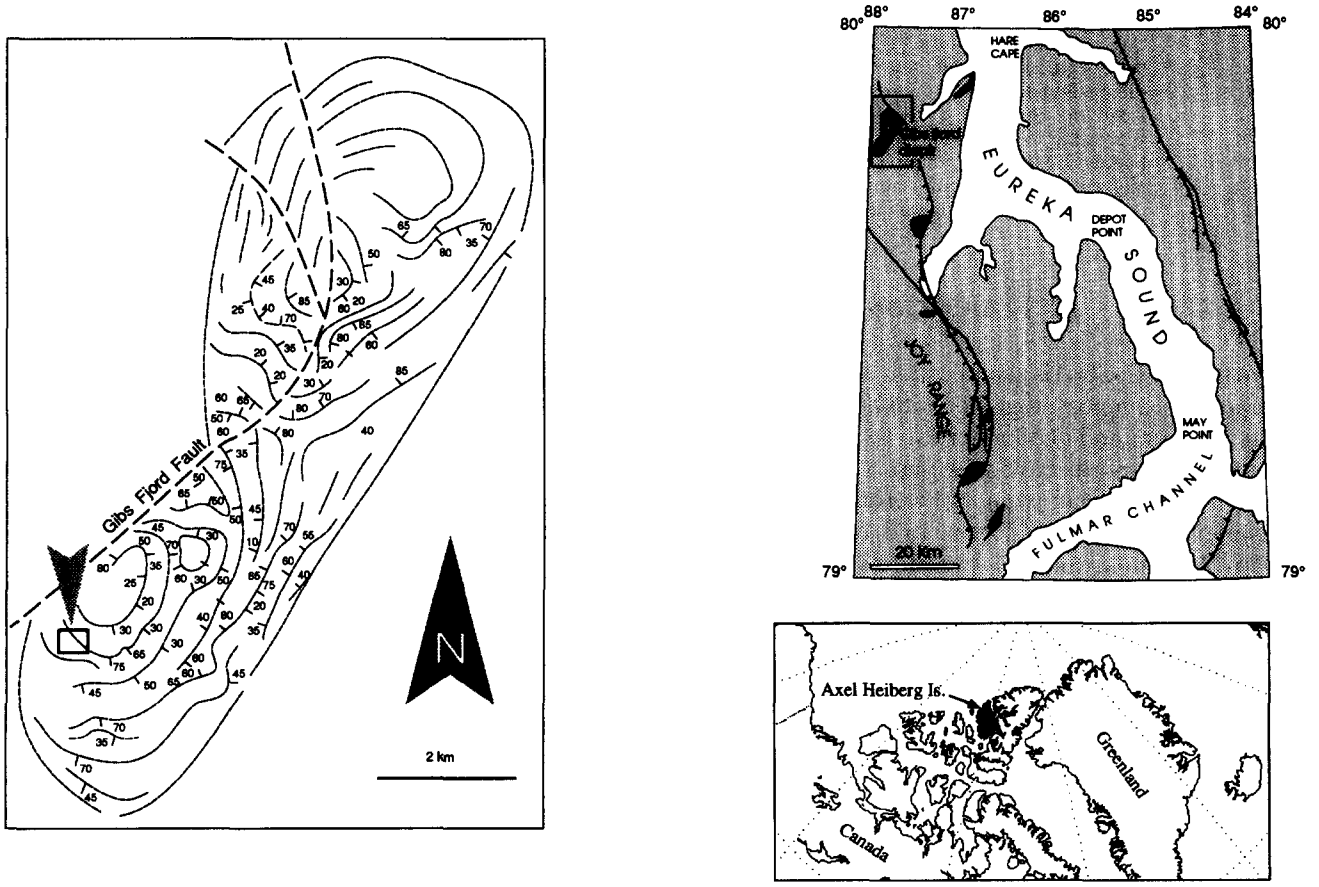

Fig. 1. Location maps of Gibs Fjord Diapir, Axel Heiberg Island, N.W. Territories, Canada (slightly modified after van Berkel *et al.* 1983). Specimen location marked by an open square and arrow.

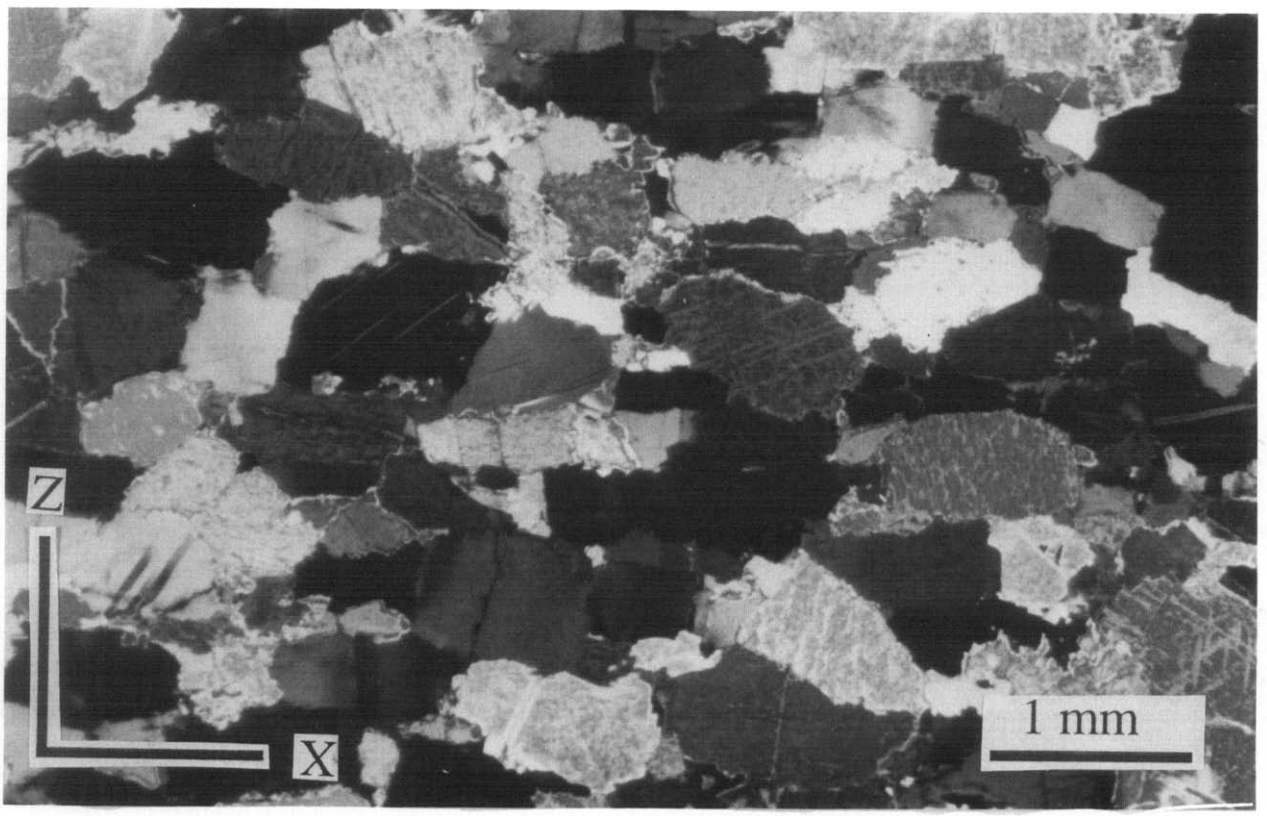

Fig. 2. Photomicrograph of the studied deformed anhydrite in the XZ structural section. Scale bar represents 1 mm.

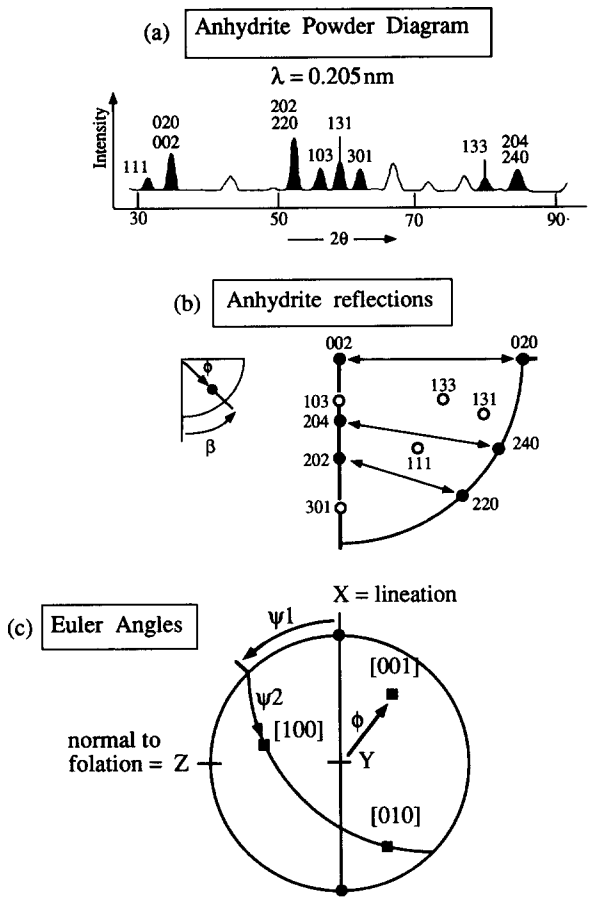

Fig. 3. Neutron texture goniometry experimental data and Euler angle conventions. (a) Neutron powder diagram at a wavelength of 0.205 nm. Shaded peaks were used in this study. Note coincidence for 020/002, 202/220 and 204/240. See Table 1 for further information. (b) Crystallographic elements of the measured pole figures. Open circles represent single reflections, filled circles are the coincident reflections. The definitions of the angles ϕ and β reported in Table 1 are also shown. (c) Conventions for structural frame X–Y–Z and Euler angles used in this study. X is parallel to the lineation and the N–S line is the foliation plane. Note XYZ are not used in the mathematical definition of the Euler angles. All pole figures are reported in the orientation.

2θ peaks. The specimen was a cylinder 10 mm in diameter and 15 mm long containing over 1000 grains of 1 mm^3 in volume.

Anhydrite has orthorhombic crystal symmetry belonging to point group mmm. The standard setting (or orientation) used to describe the structure is space group Cmcm. However, due to confusion caused by the crystal axes of similar lengths, and the preference of various authors, three different space groups Bbmm (e.g. Höhne 1963), Amma (e.g. Cheng & Zussman 1963, Kirfel & Will 1980) and Bmmb (e.g. McMurdie *et al.* 1986, Hartman 1989) have been used to illustrate the structure. Here we will adhere to the Bbmm space group, hence conforming with all the fabric studies previously cited, with crystal axes $a = 0.6238$ nm $< b = 0.6992$ nm $< c = 0.6998$ nm, the axial lengths being the average three recent determinations given by Hartman (1989). To a very good approximation we can consider the structure to have $a < b = c$, hence reflections (hkl) and (hlk) to be in perfect coincidence. In the following texture analysis we have used this approximation in using the harmonic pole figure inversion method of Bunge & Wenk (1977) to resolve these coincidences.

The orientation distribution function (ODF), is a function f(**g**) that quantitatively describes the volume fraction of the sample with an orientation **g**. The advantage of the ODF for fabric analysis is that one has the complete orientation, and can calculate pole figures of elements that cannot be measured directly, e.g. the (100) pole figure of anhydrite. The function f(**g**) is given in terms of symmetrical generalized harmonics (Bunge 1982) and is defined in equation (1) as:

$$\mathrm{f}(\mathbf{g}) = \sum_{l=0}^{L_{max}} \sum_{m=1}^{M(l)} \sum_{n=1}^{l} C_l^{mn} T_l^{mn}(\mathbf{g}), \qquad (1)$$

where C_l^{mn} are the coefficients of the series development of the texture function f(**g**); T_l^{mn} (**g**) are the generalized spherical harmonic functions; $M(l)$ is the number of linearly independent harmonics and L_{max} is the maximum degree used in the expansion. The eight 2θ peaks, corresponding to the measured pole figures were indexed in the Bbmm group as shown in Fig. 3 (see Table 1). Perfect coincidences occur for (020)/(002), (202)/(220) and (204)/(240). With eight experimental pole figures the harmonic inversion was performed with a triclinic sample and orthorhombic crystal symmetry. We used a FORTRAN program (Casey 1981), to perform the inversion with a truncation value of $L_{max} = 14$. The experimental pole figures intensities $I_{expt}(h)$ in direction h were compared with calculated pole figures (Fig. 4) intensities, $I_{calc}(h)$, using an absolute error parameter (ERN) defined in equation (2) which was introduced by Wagner & Humbert (1987):

$$\mathrm{ERN} = \frac{100}{n} \sum_{h} |I_{expt}(h) - I_{calc}(h)| \quad , \qquad (2)$$

where n is the number of measurement points. The (301) pole figure has the highest error at 8.7% and (133) the lowest at 5.4%. The pole figures with coincident reflections are in the middle range of the error parameter.

The experimental and calculated pole figures are presented in Fig. 4. The calculated pole figures reproduce all the features present in the experimental pole figures with a slightly smoothed topology. In addition we

Table 1. Crystallographic data for pole figures of anhydrite, see Fig. 3 for the definition of β and ϕ

2θ (expt)	2θ (calc) $\lambda = 0.205$ nm	hkl	β	ϕ	Relative intensity
30.7	30.67	111	41.7	56.4	1.00
34.1	34.08	002	0.0	0.0	0.49
	34.10	020	90.0	90.0	0.51
52.3	52.25	202	0.0	48.3	0.62
	52.26	220	41.7	90.0	0.38
56.1	55.97	103	0.0	20.5	1.00
59.0	58.93	131	69.5	72.7	1.00
62.0	61.90	301	0.0	73.5	1.00
80.2	80.06	133	69.5	46.9	1.00
84.6	84.43	204	0.0	29.3	0.61
	84.48	240	60.7	90.0	0.39

have calculated the separated coincident pole figures (020)/(002), (202)/(220) and (204)/(240). In the case of (020) and (002) the distinct almost equal intensity contributions (51.4 vs 48.6%, see Table 1) to experimental pole figure are clearly revealed (Fig. 5). A strong maximum (6.3 multiples of a uniform distribution, m.u.d.) of (020) is calculated to be near the lineation (X) and $\perp$(002) forms a girdle normal to the lineation (YZ plane) with a maximum (4.0 m.u.d.) normal to the foliation (Z). The results for (202) and (220) illustrate the relative contributions of each to the experimental pole figure, but in this case (202) contributed 62.3% to the intensity compared to only 37.7% for (220). Finally (204) and (240) show the much greater importance of (204) (61.1 vs 38.9%) to the observed topology of the experimental pole figure.

The Euler angles (Bunge 1982) are used to describe the ODF in a manner illustrated in Fig. 3. The ODF is

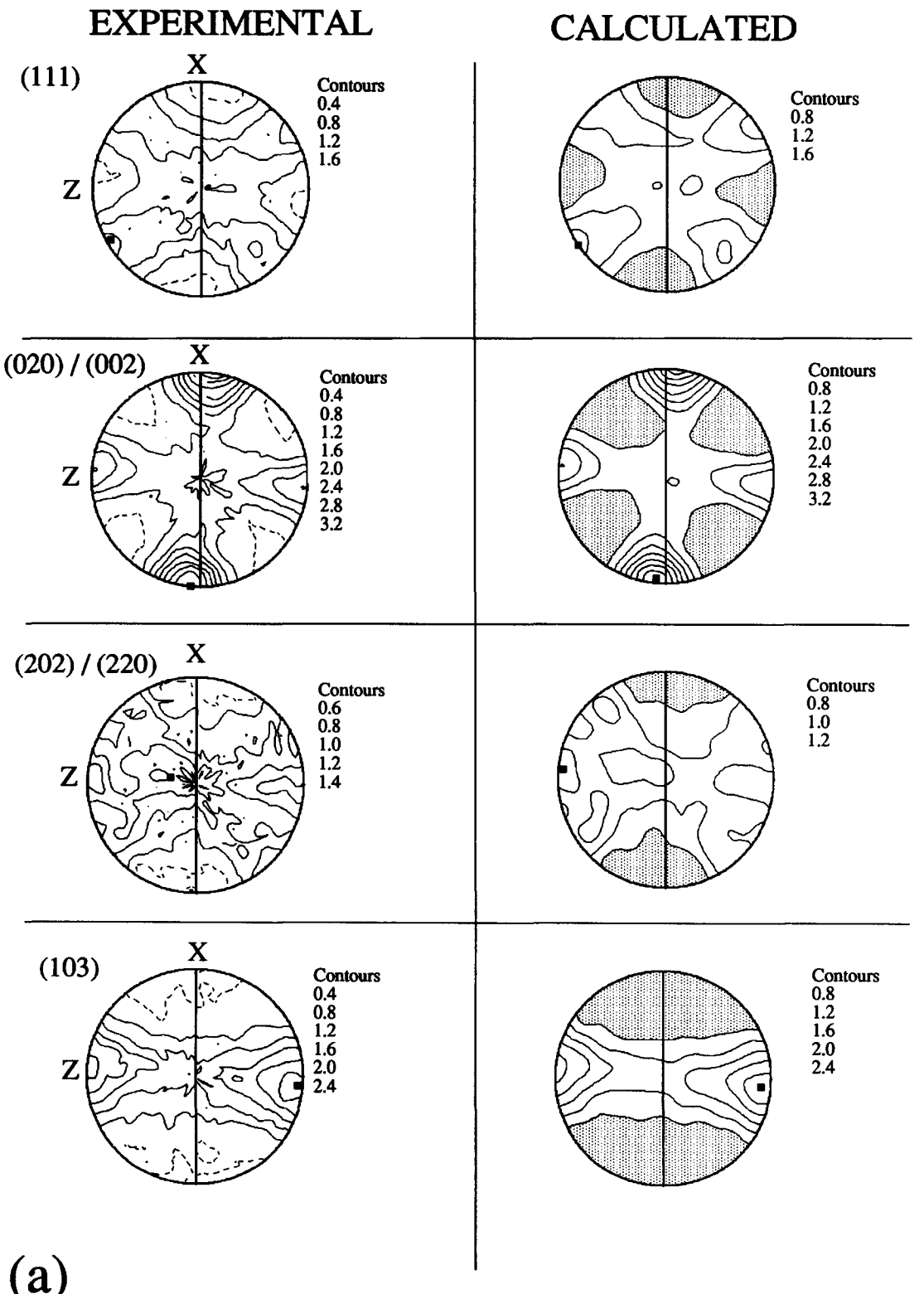

Fig. 4(a).

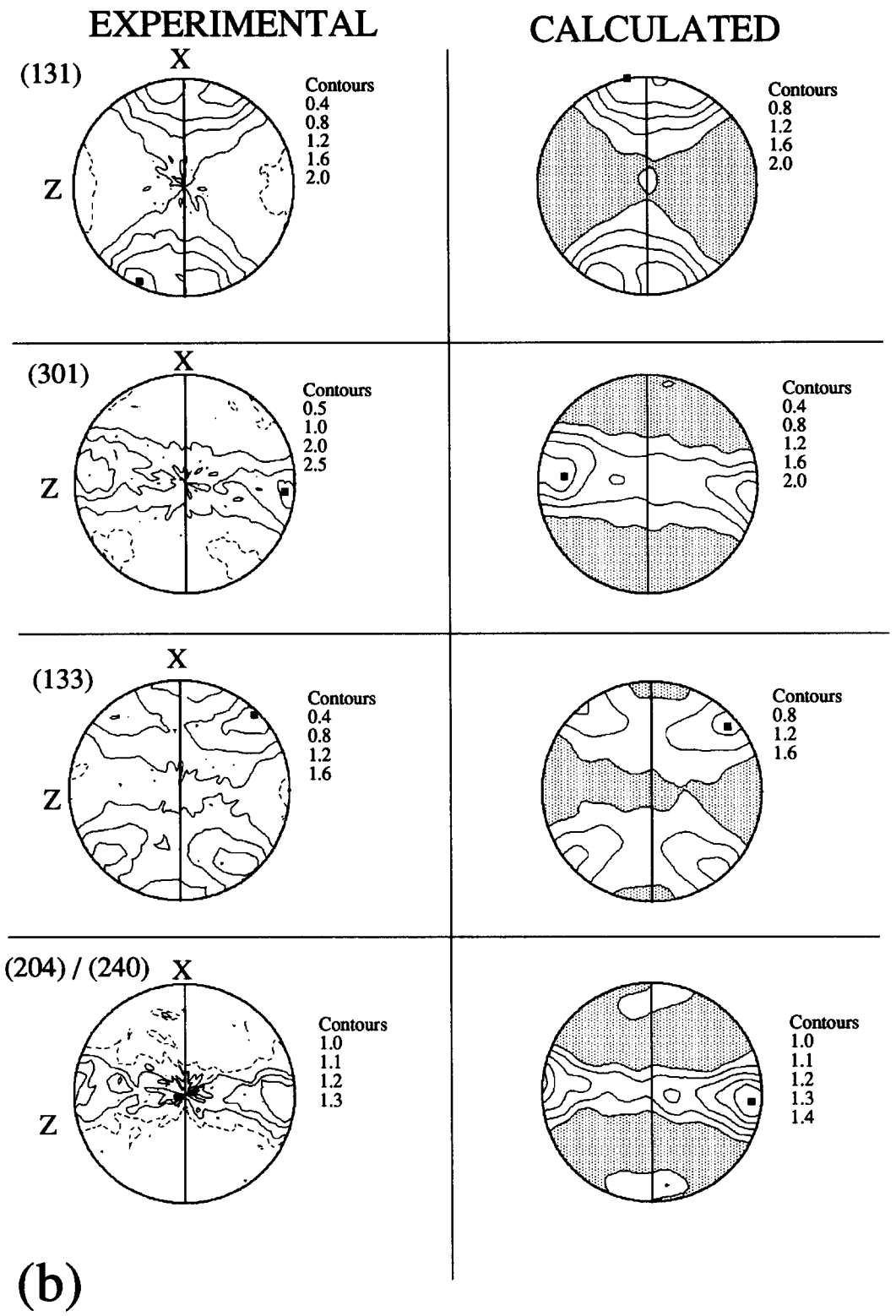

Fig. 4. Experimental and calculated pole figures from the ODF coefficients, contoured in multiples of a uniform distribution (m.u.d.). Harmonic expansion of the pole figure coefficients truncated at $L = 14$. Lowest contour is a dashed line in the experimental pole figures. Regions with densities below lowest contour shaded in calculated pole figures. Black square indicates the orientation with the highest density in all pole figures. (a) Pole figures (111),(020)/(002),(202)/(220) and (103). (b) Pole figures (131),(301),(133) and (204)/(240).

presented as three sections (Figs. 6a–c), two containing the maximum density of 8.9 m.u.d. at E ($\psi_1 = 170°$, $\phi = 90°$, $\psi_2 = 90°$; Figs. 6a&b). The main feature of the ODF is a high density tube-like structure at $\psi_2 = 90°$ which extends from $\phi = 0°$ to 180° (marked A–B in Fig. 6a). In the $\phi = 90°$ section the A–B tube (marked E in Fig. 6b) can be seen in section as two high density regions at $\psi_1 =$ 0–10° and 170–180° which represent a single physical orientation. The tube structure represents an axial fabric distribution about [010]. The axial symmetry is well illustrated by the (020) and (002) pole figures (Fig. 5), where the symmetry axis is parallel to the specimen X

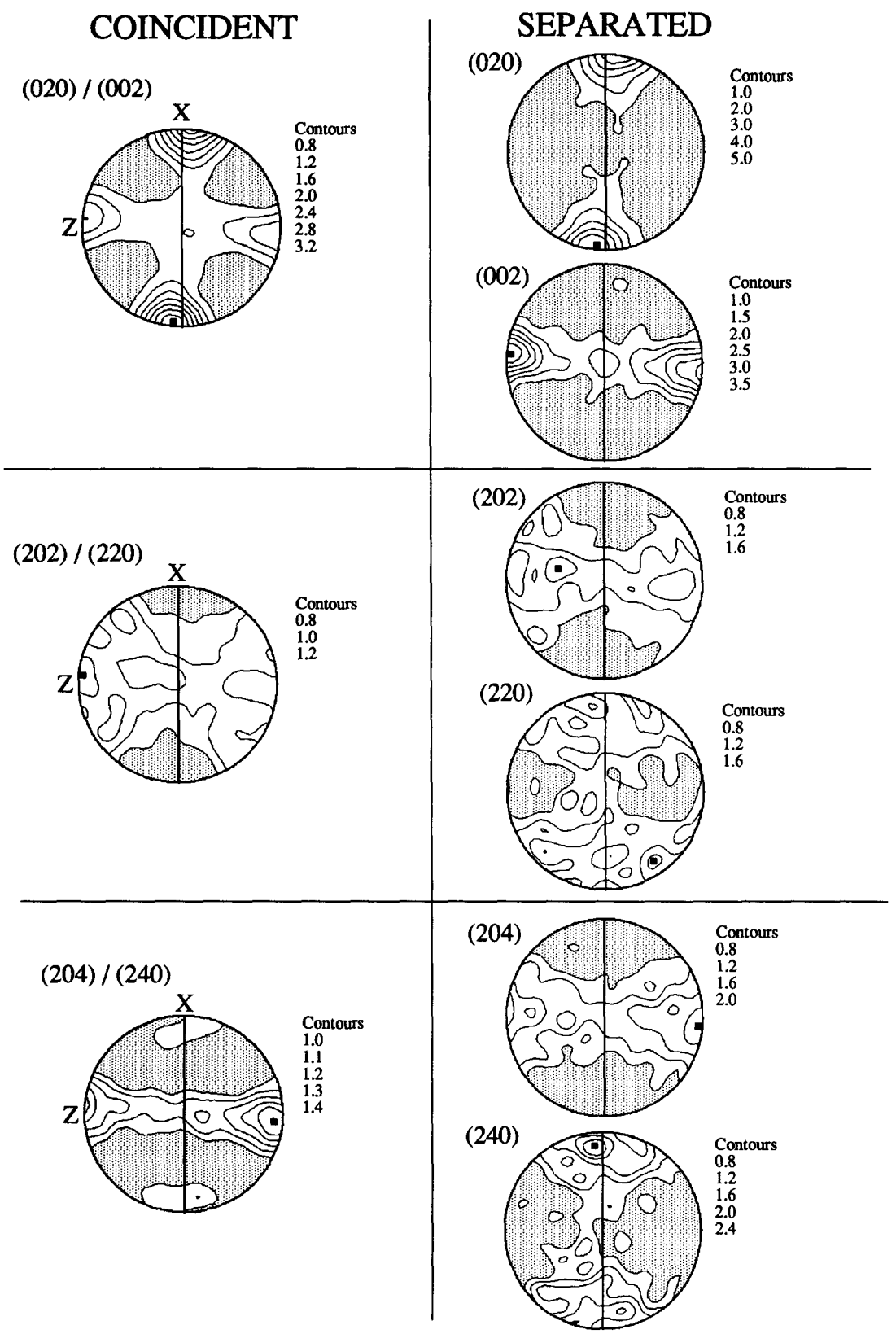

Fig. 5. Coincidence and separated pole figures, both calculated from the ODF coefficients with a harmonic expansion truncated at $L = 14$. Regions with densities below lowest contour shaded. Black square indicates the orientation with the highest density.

axis, (020) forms a point maximum parallel to X and (002) a girdle normal to X in the YZ plane. Point E (Figs. 6a&b) in the ODF tube has the orientation most characteristic of the texture with [010] parallel to X and [001] parallel to Z (Figs. 6a&b). There is a second important orientation at B ($\psi_1 = 170°$, $\phi = 180°$, $\psi_2 = 90°$; Figs. 6a&c) with a density of 8.3 m.u.d., which is at one end of the high density tube A–B. The B orientation

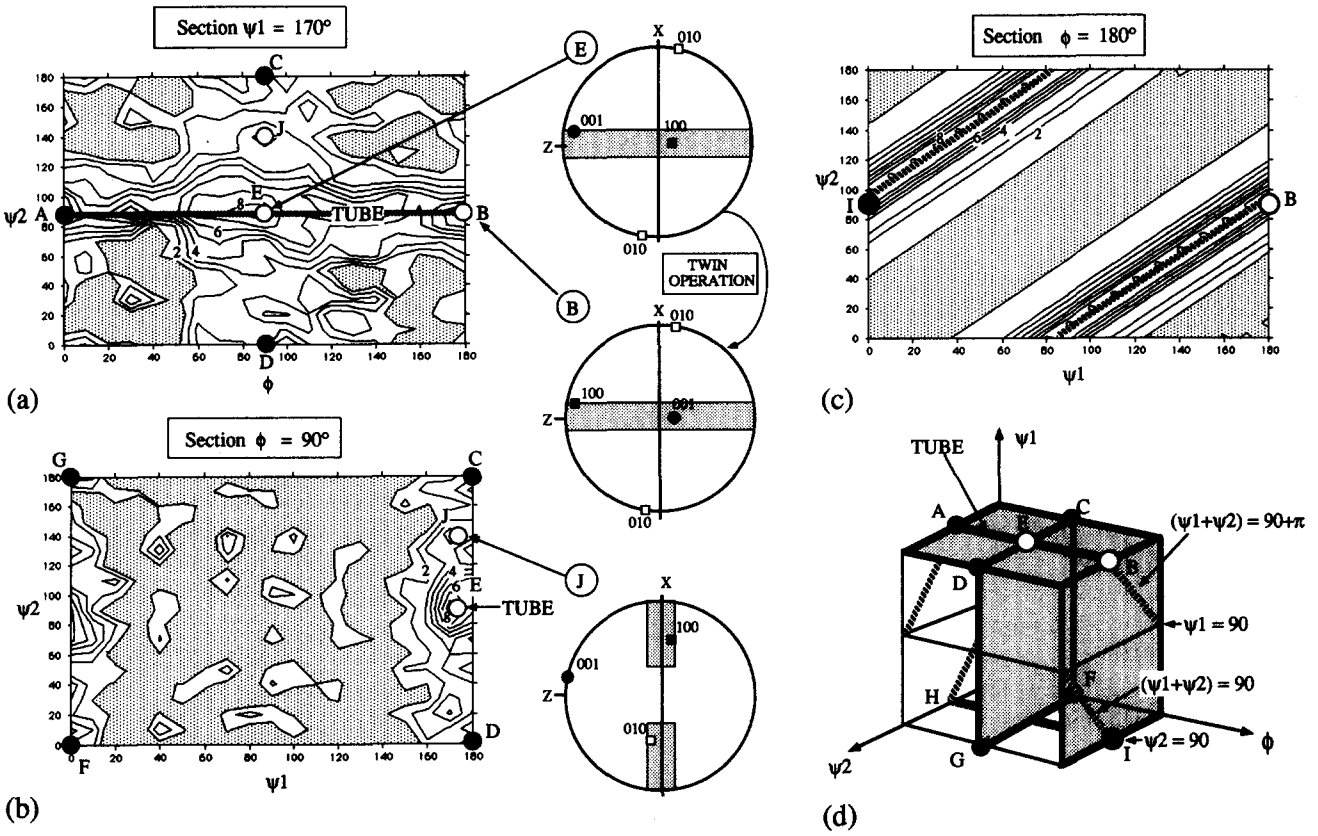

Fig. 6. ODF sections of the even function at $\psi_1 = 170°$, $\phi = 90°$ and $\phi = 180°$ and summary block diagram. The regions below 1 m.u.d. have been shaded. Harmonic expansion truncated at $L = 14$. Letters B, E and J mark the orientations mentioned in the text and stereograms show the orientation of [100],[010] and [001] in structural co-ordinates XYZ (same orientation as pole figures in Figs. 4 and 5). (a) ODF section at $\psi_1 = 170°$. (b) ODF section at $\phi = 90°$. (c) ODF section at $\phi = 180°$. (d) Summary of the ODF showing the orientations of sections at $\psi_1 = 170°$, $\phi = 90°$ and $\phi = 180°$ as shaded faces with a thick black outline. Orientations B and E indicated by the white dots and reference letters for the ODF sections marked by black dots. The high density tube is shown by a grey line and the bands ($\psi_1 + \psi_2$) in the twinned orientation ([100] parallel to Z) by the striped lines.

is related to E by a 90° rotation about [010], with [100] parallel to Z. In the section $\phi = 180°$ the orientation B occurs at two high density bands (B and I in Fig. 6c) with a density of 8.3 m.u.d. The bands represent the same physical orientation as B, because when $\phi = 0°$ or 180° the crystal orientation is completely described by ($\psi_1 + \psi_2$). In the present case ($\psi_1 + \psi_2$) = 90°, or 90° + 180° as shown in Fig. 6(d), the additional 180° rotation changes the sign of [100] at Z. The orientations E and B are the main features of the texture. In the section $\psi_1 = 170°$ (Fig. 6a) there is a second tube-like structure marked by the letters C–D at $\phi = 90°$. The C–D structure is wider and less dense than the A–B tube. This structure is caused by distribution of [100] and [010] axes in the foliation (XY) plane, as illustrated by the orientation at J ($\psi_1 = 170°$, $\phi = 90°$, $\psi_2 = 140°$; Figs. 6a&b) with a density of 4.9 m.u.d. The second tube C–D is a minor volume fraction of the overall texture as it is not seen in other ODF sections. A summary of the main features of the ODF are given in Fig. 6(d).

Inverse pole figures (IPF) have been calculated for the two principal structural directions, i.e. parallel to the lineation (X) and normal to the foliation (Z). The IPF for the X direction (Fig. 7) shows the major concentration of X close to [010], similar information is given in

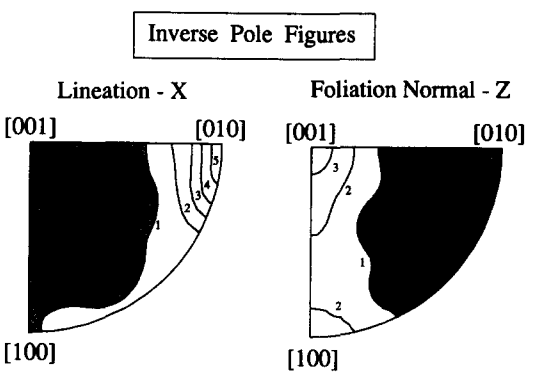

Fig. 7. Inverse pole figures calculated from the ODF coefficients ($L = 14$), for the directions parallel to the lineation (X) and normal to the foliation (Z). The regions below 1 m.u.d. have been shaded.

the (020) pole figure with a point maximum close to X (Fig. 5). The IPF for the Z direction shows the high concentration of Z close to [001] (3.5 m.u.d.) and [100] (2.5 m.u.d.) with a ridge of high concentration joining [001] and [100] (>1.0 m.u.d.). The (002) pole figure contains identical information, namely a maximum concentration at Z and a girdle normal to X in the YZ plane (Fig. 5). A strong axial symmetry about [010] is evident in the IPF for the Z direction.

DISCUSSION

Previous microstructural and petrofabric studies of experimentally deformed anhydrite have established the following mechanisms (Müggе 1883, Ramez 1976a).

(1) Translation glide on (001) [010].

(2) Translation glide on {012} in $[\bar{1}2\bar{1}]$ and $[1\bar{2}1]$ in the positive sense only.

(3) Twinning on {101} in a direction parallel to the intersection of (101) and (010) in a negative sense.

Contrary to the usual experience in metals, slip occurs at all temperatures, whereas deformation twinning is only active at high temperatures (>300°C) at experimental strain rates (Ramez 1976a, Müller *et al.* 1981).

The general characteristics of the fabric patterns of naturally deformed anhydrite rock determined by optical techniques has been summarized by Kern & Richter (1985) as follows:

(1) a pronounced maximum of [010] parallel to the lineation and a weak submaximum perpendicular to it in the foliation plane;

(2) [100] and [001] forming girdles normal to the [010] maximum which includes maxima of variable orientations.

The quantative lattice preferred orientation (texture) measurements we have made confirm the general trends obtained by the previous optical studies. The question remains what were the deformation mechanisms that produced these fabric patterns? The microstructural data are as follows:

(1) a few twin lamellae per grain;

(2) grains having straight boundaries, with only occasional serrated grain boundaries observed;

(3) grains are elongated along [010] with undulatory extinction.

This microstructure is similar to that observed by Müller *et al.* (1981) (see their fig. 8) for an experimentally deformed sample (350°C, 5×10^{-6} s^{-1}, 25% axial shortening) which was subsequently annealed for 7 h at 450°C. Further, their experiments showed that annealing did not change the characteristics of the deformation fabric, although it was weakened. Although *a priori* we do not know the orientation of the stress tensor during the natural deformation, nor the strain path to which the specimen was subjected, it is reasonable to assume the principal compressive stress (σ_1) was close to the foliation normal (Z). Given that assumption it is interesting that we observe a maximum in the IPF for the Z direction at [100] (Fig. 7), similar to the experimentally deformed samples where twinning was an active mechanism (Ramez 1976a,b, Müller *et al.* 1981). The calculated pole figure of the twin plane {101} (Fig. 8) shows a strong concentration at ~45° to Z, the ideal orientation for deformation by twinning.

Having established twinning as a component to the deformation mechanism responsible for the fabric development, what can we deduce about the relative activity of the glide mechanisms? The strong maximum of [010] parallel to the lineation and the girdle of ⊥(001) with a maximum normal to the foliation (Z), together with elongation of grains parallel to [010], are indicative of (001) [010] translation glide. We note that [010] and ⊥(001) are slightly offset (asymmetric) with respect to the structural frame (X–Y–Z) which is typical of low symmetry minerals deformed in a non-coaxial regime (e.g. Bouchez & Duval 1982). In a non-coaxial deformation, such as simple shear, we expect the axis of external rotation (AER) for the dominant slip system to remain in a fixed orientation near the intermediate strain axis (Y) at high strains. In the case of (001)[010] slip the AER, the axis which is normal to the slip direction [010] and the slip plane normal ⊥(001), are all the [100] axis. The [100] axis has a subsidiary maximum normal to lineation in the foliation plane (Y) of 1.8 m.u.d. (Fig. 8). A contribution to fabric development by $[\bar{1}2\bar{1}]\{012\}$ and $[1\bar{2}1]\{012\}$ allows the activation of more than the five independent slip systems required by the von Mises criteria for a general constant volume deformation. The AER for this slip system is ⊥(521) about 22° from the [100] axis, the (521) pole figure is very similar to (100) (Fig. 8), hence it is difficult to distinguish between these two slip systems using the AER. The intensity in the (521) pole figure is lower (1.2 m.u.d.) than (100) at Y, and we suggest that (001)[010] was the dominant glide system.

It is difficult to estimate the relative contributions of twinning and glide to the fabric development because twinning can be such an efficient mechanism for transferring volume fraction of the sample to the twinned orientation (Müller *et al.* 1981) for a given strain. Complete twinning may only represent 20% shortening (Müller *et al.* 1981), hence one should be careful not to over estimate its importance as strain accommodation mechanism, however it may be very important for fabric development. The volume fraction in the twinned orientation is given by all the orientations with their [100] axes parallel to Z; in the ODF these orientations are seen in the sections with $\phi = 0°$ or 180° with $\psi_1 + \psi_2 = 90°$ or 90° + 180°. If we sum the volume fraction of all the orientations with [100] within 10° of Z we find that 34.1% of the ODF is in the twinned orientation. One can put forward a symmetry argument to suggest that glide is the more important mechanism for fabric development, in particular [010](001). All pole figures show an axial symmetry about X (lineation), which coincides with the strong point maxima for (020). The importance of this axial symmetry is further emphasised by the tube-like structure of the ODF (Fig. 6), this is the major symmetry element of the ODF. Such a distribution would be produced by [010](001) in an axial extension parallel to X. However the axial symmetry is not perfect as illustrated by the density variations of the ODF tube structure, which corresponds to scatter about two dominant orientations, the glide orientation E ($\psi_1 = 170°, \phi = 90°, \psi_2 = 90°$) for [010](001) and the twinned orientation B. The {101} twin rotates the [001] of twinned domain by 83.5° about [010] (Klassen-Neklyudova 1964), almost identical to the observed rotation between orientations E and B. The volume fraction transfer in the ODF between glide (E) and twinned (B) orientations

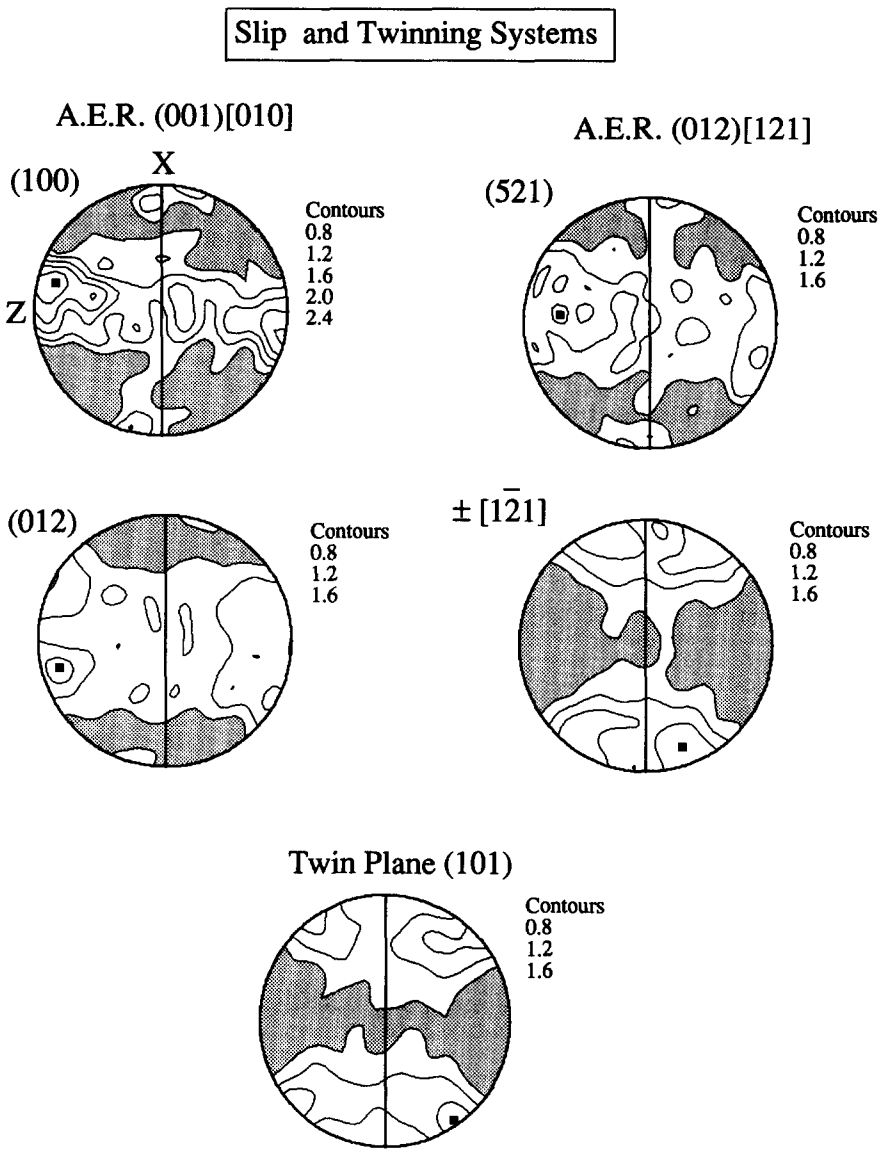

Fig. 8. Pole figures of slip twinning systems calculated from the ODF coefficients for ⊥(100) the axis of external rotation (AER) for [010](001), ⊥(521) the AER for [1$\bar{2}$1](012), ⊥(012), ± [1$\bar{2}$1] and the twin plane ⊥(101). Regions with densities below lowest contour shaded. Black square indicates the orientation with the highest density.

(Figs. 6a&b) results in an axial fabric about X (ODF tube in Fig. 6). Hence the interaction between glide and twinning is partly responsible for the axial symmetry about [010] or X, for example transferring [100] axes from X to Z. If twinning was the dominant process for the fabric development we would expect an axial symmetry about the maximum compressive stress direction or a (point) maximum in the (100) pole figure near Z. No axial symmetry about Z is observed, hence we conclude that glide was the dominant deformation mechanism, but that twinning has made volumetrically important contribution (30%) which may not represent a large strain. The combination of glide and twinning resulted in an axial fabric about the X axis.

CONCLUSIONS

Neutron diffraction texture goniometry allows a quantative analysis of the texture of a naturally deformed coarse-grained anhydrite. The calculation of the ODF by pole figure inversion provides a method of analysis in the present case of overlapping pole figures, where $\{hkl\}$ 2θ peak coincides with $\{hlk\}$. The ODF reveals that there is a strong concentration of [100] axes close to foliation normal (Z), rather than the Y specimen axis as might have been suspected from the measured (020)/(002) pole figure.

The deformation mechanisms that produced the fabric is interpreted to be a combination of glide on (010) and (012), and twinning on (101). The dominant mechanism appears to be [010](001) glide in a non-coaxial flow regime. The symmetry of the ODF and pole figures suggests a strong component of axial extension parallel to the lineation (X). Deformation twinning, a relatively high temperature deformation mechanism in anhydrite at laboratory strain rates, has played a secondary role as a strain accumulation mechanism, but has left a strong imprint on the fabric as it was partly responsible for the axial symmetry about X. The high temperature nature of

deformation is consistent with the microstructure which consists of grains with straight and occasional serrated boundaries. We interpret the increased frequency of twinning and recrystallization with increasing temperature (above 300°C) at laboratory strain rates and the presence of this microstructure at natural strain rates to indicate that there is a thermally activated nucleation to the twinning process, for example by nucleation at migrating grain boundaries. The volumetrically quantitative neutron texture analysis is particularly well suited to studying samples deformed by twinning because volume fractions (host/twin) are often impossible to evaluate by traditional optical techniques. The interactions of glide, recrystallization and twinning will therefore require careful consideration before anhydrite fabric development can be modelled using the numerical simulation techniques.

Acknowledgements—The authors thank the Laboratoire Léon-Brillouin, C.E.N., Saclay for access to the neutron diffraction facilities and W. M. Schwerdtner for his constructive comments on the manuscript. J.-L. Bouchez would like to thank the Polar Continental Shelf Project and W. M. Schwerdtner's team for logistic support on Axel Heiberg Island.

REFERENCES

Balk, R. 1949. Structure of Grand Saline salt dome, van Zandt County, Texas. *Bull. Am. Ass. Petrol. Geol.* **33**, 1791–1829.

Bouchez, J.-L. & Duval, P. 1982. The fabric of polycrystalline ice deformed in simple shear-experiments in torsion, natural deformation and geometrical interpretation. *Textures & Microstruct.* **5**, 171–190.

Bunge, H. J. 1982. *Texture Analysis in Materials Science*. Butterworth, London, 593.

Bunge, H. J. & Wenk, H. R. 1977. Three-dimensional texture analysis of three quartzites (trigonal crystal and triclinic specimen symmetry). *Tectonophysics* **40**, 257–285.

Cahn, R. W. 1983. Recovery and Recrystallization. In: *Physical Metallurgy* (3rd edn) (edited by Cahn, R. W. & Haasen, P). North-Holland, Amsterdam. 1596–1672.

Casey, M. 1981. Numerical analysis of X-ray texture data: an implementation in FORTRAN allowing triclinic or axial specimen symmetry and most crystal symmetries. *Tectonophysics* **78**, 51–64.

Cheng, G. C. H. & Zussman, J. 1963. The crystal structure of anhydrite ($CaSO_4$). *Acta Cryst.* **16**, 767–769.

Hartman, P. 1989. On the unit cell dimensions and bond lengths of anhydrite. *Eur. J. Mineral.* **1**, 721–722.

Hawthorne, F. C. & Ferguson, R. B. 1975. Anhydrous sulphates. II. Refinement of crystal structure of anhydrite. *Can. Mineral.* **13**, 289–292.

Höhne, E. 1963. A more accurate determination of the crystal structure of anhydrite. *Sov. Phys.-Crystallogr.* **7**, 559–569.

Jordan, P., Noack, T. & Widmer, D. 1990. The evaporite shear zone of the Jura Boundary Thrust—new evidence from Wisen well (Switzerland). *Ecolog. geol. Helv.* **83**, 525–542.

Kern, H. & Richter, A. 1985. Microstructures and textures in evaporites. In: *Preferred Orientation in Deformed Metals and Rocks* (edited by Wenk, H.-R.). Academic Press, Orlando. 317–333.

Kirfel, A. & Will, G. 1980. Charge density in anhydrite, $CaSO_4$, from X-ray and neutron diffraction measurements. *Acta Cryst.* **B36**, 2881–2890.

Klassen-Neklyudova, M. V. 1964. *Mechanical Twinning of Crystals*. Consultants Bureau, New York, 87.

Lamcke, K. 1936. Gefügeanalytische Untersuchungen am Anhydrit nebst einem Beitrag zu den optischen und röntgenographischen Methoden der Gefügeanalyse. Unpublished dissertation, University of Kiel.

McMurdie, H., Morris, M. C., Evans, E. H., Paretzkin, B., Wong-Ng, W. & Hubbard, C. R. 1986. Standard X-ray diffraction powder patterns from the JCPDS research associateship. *Powder Diffract.* **1**, 265–275.

Morikawa, H., Minato, I., Tomita, T. & Iwai, S. 1975. Anhydrite: a refinement. *Acta Cryst.* **B31**, 2164–2165.

Mügge, O. 1883. Über Translationen und verwandte Erscheinungen in Kristallen. *Neues Jb. Miner.* **1**, 71–162.

Müller, P. & Siemes, H. 1974. Festigkeit Verformbarkeit und Gefügeregelung von Anhydrit. *Tectonophysics* **23**, 105–127.

Müller, W. H., Schmid, S. M. & Briegel, U. 1981. Deformation experiments on anhydrite rocks of different grain sizes: Rheology and microfabrics. *Tectonophysics* **78**, 527–543.

Ramez, M. R. H. 1976a. Mechanisms of intragranular gliding in experimentally deformed anhydrite. *Neues Jb. Miner.* **127**, 311–329.

Ramez, M. R. H. 1976b. Fabric changes in experimentally deformed anhydrite rocks. *Neues Jb. Miner.* **128**, 89–113.

Schwerdtner, W. M. 1964. Gerfügestudien an Anhydritbänken im Benther Saltzstock (Werk Ronnenberg). *Kali Steinsalz* **4**, 64–70.

Schwerdtner, W. M. 1970. Lattice-orienting mechanisms in schistose anhydrite. In: *Experimental and Natural Rock Deformation* (edited by Paulitsch, P.). Springer, Berlin. 142–162.

van Berkel, J. T., Hugon, H., Schwerdtner, W. M. & Bouchez, J.-L. 1983. Study of anticlines, faults and diapirs in the central Eureka Sound fold belt, Canadian Arctic Islands: Preliminary results. *Bull. Can. Petrol. Geol.* **32**, 343–358.

Wagner, F. & Humbert, M. 1987. Texture analysis from incomplete pole figures in low symmetry cases. *Textures & Microstruct.* **7**, 115–129.